Proton Testing Results for Kaman KD-5100 Differential Inductive Position Measuring Systems

Bart H. McGuyer, Randall J. Milanowski, Slaven Moro, Norman Hall, and Bert Vermeire

***Abstract*—We report proton testing of a position measuring system, the Kaman KD-5100, with applications including mirror positioning for laser beam control. We measure a device response likely due to total ionizing dose and/or displacement damage.**

I. Introduction

Accurately and precisely measuring position is challenging in high-radiation environments. While radiation-hardness-assured position sensing systems exist, their high cost and long lead times are prohibitive for many applications. Here, we consider a commercial position sensing system, the KD-5100 by Kaman Precision Products [1], which has a decades-long history of use in military and industrial applications that require high precision and high reliability, for example, with active mirrors for laser beam steering [2]–[4]. However, while the KD-5100 has been successfully used in high-radiation environments [1], little information is available about its performance and degradation after irradiation.

Here we present the results of irradiating a KD-5100 system with 64 MeV protons to a total fluence of 8.6×10^{11} protons/cm^2 at the University of California, Davis, Crocker Nuclear Laboratory (CNL). The corresponding total ionizing dose (TID) from the CNL facility dosimetry was 115.7 kRad(Si). Proton irradiation was used to simultaneously impart non-ionizing (displacement damage) and ionizing (total dose and transient) radiation effects, both of which may be present in the KD-5100 system. Stopping and range of ions in matter (SRIM) analysis estimated that the proton energy was attenuated by about 5 MeV by the metal case and packaging construction, and that the 59 MeV protons remaining after this attenuation were sufficient to penetrate the active component region. We expect that these results will be of use to the satellite and aerospace industries and will move forward Facebook's mission of connectivity.

Manuscript received July 11, 2017.

B. H. McGuyer is with Facebook Inc., 1 Hacker Way, Menlo Park, CA 94025, USA.

R. J. Milanowski is with M&A Inc., 2726 Shelter Island Drive #268, San Diego, CA 92016, USA.

S. Moro is with Facebook Inc., 1 Hacker Way, Menlo Park, CA 94025, USA.

N. Hall is with Space Micro Inc., 10237 Flanders Court, San Diego, CA 92121, USA.

B. Vermeire is with Space Micro Inc., 10237 Flanders Court, San Diego, CA 92121, USA.

978-1-5090-4647-8/17/$31.00 ©2017 IEEE

II. Part Description and Experimental Approach

The KD-5100 is a high-precision non-contact position measuring system with two measurement channels (or axes). Each channel uses a pair of matched inductors as differential sensors to measure the linear displacement or angular tilt of a metal target. The impedance of each sensor depends on the proximity to its target, primarily because inducing eddy currents reduces each sensor's self inductance. The system measures these impedance changes using an alternating-current balanced bridge circuit, similar to a Wheatstone bridge. The bridge output is demodulated and amplified to provide an analog signal that is very nearly linear with changes in the target position. The KD-5100 accomplishes these functions using circuitry that includes diodes and bipolar components.

Fig. 1 shows the test system used at CNL. For each mea-

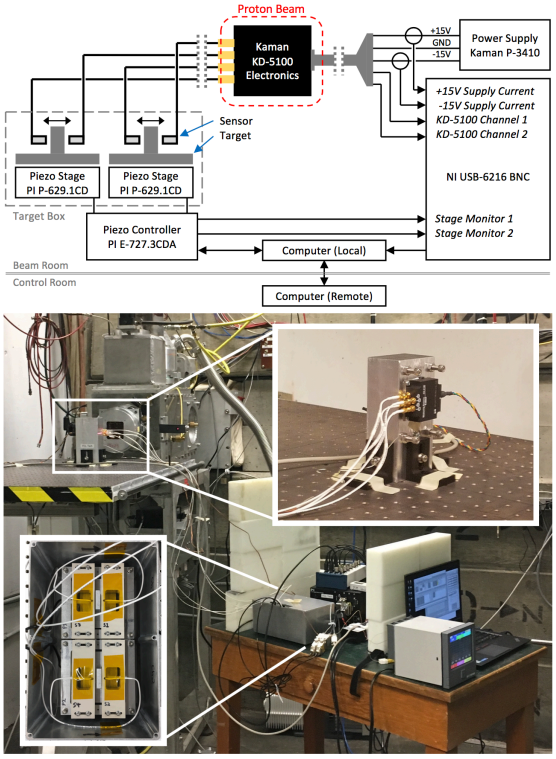

Fig. 1. (Top) Diagram of the test system. (Bottom) Picture of the test system setup in the Crocker Nuclear Laboratory north cave. Insets highlight the device under test and show the components inside the target box.

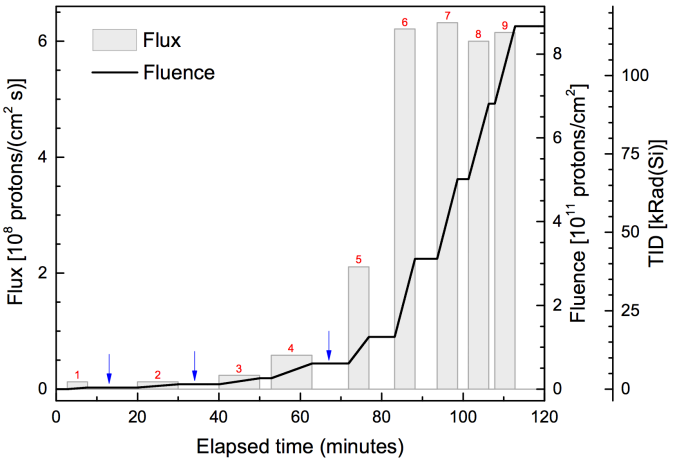

Fig. 2. Flux $\phi(t)$ and total fluence $\Phi(t) = \int_0^t \phi(\tau)d\tau$ versus time for the irradiation of the device under test by 64 MeV protons in nine exposure runs. An additional axis for the fluence shows the total imparted TID as measured by CNL facility dosimetry [10^{12} protons/cm^2 corresponds to about 134 kRad(Si)]. Red numbers label each exposure run. Blue arrows mark when calibration data sets were taken in between exposures. Additional calibration data sets were taken before and after all irradiation. Monitoring data sets were taken during all exposures.

surement channel of the KD-5100 device under test (DUT), the sensor pair was placed on opposite sides of an aluminum target that was controlled by a linear piezo stage. Each piezo stage provided precise control of its target position, and included a capacitive sensor to directly measure its target position. Each sensor pair was installed by offsetting one sensor from a centered target with a precision metal shim, and then adjusting the other sensor to produce a null output [5]. A computer in the CNL north cave (beam room) controlled the piezo stages and recorded the DUT channel outputs, DUT power supply currents, and piezo stage position monitors (capacitive sensor outputs). A separate computer in the CNL south cave (control room) was used to remotely control and monitor the entire test system.

We performed two types of measurements on the DUT at room temperature: active calibration and passive monitoring. During calibration, the piezo stages were discretely stepped over a range of 1.5 mm for two to three periods of a triangle wave. The data recorded during a calibration provides a comparison of the DUT outputs and piezo-stage sensor outputs, which we use to assess the DUT performance over nearly all of its measurement range. During monitoring, the piezo stages are held fixed by a piezo controller. The target for the first channel is held near one end of full scale, and the target for the second near null. This arrangement makes the first channel mainly sensitive to changes in its gain adjustment, and the second channel mainly sensitive to changes in its null adjustment. Switching between calibration and monitoring lead to slight technical offsets in the piezo controller behavior, which resulted in each calibration data set using slightly offset sweep ranges and each monitoring data set using slightly different fixed positions. These offsets are not from irradiation, and did not affect the fidelity of the piezo-stage monitor signals.

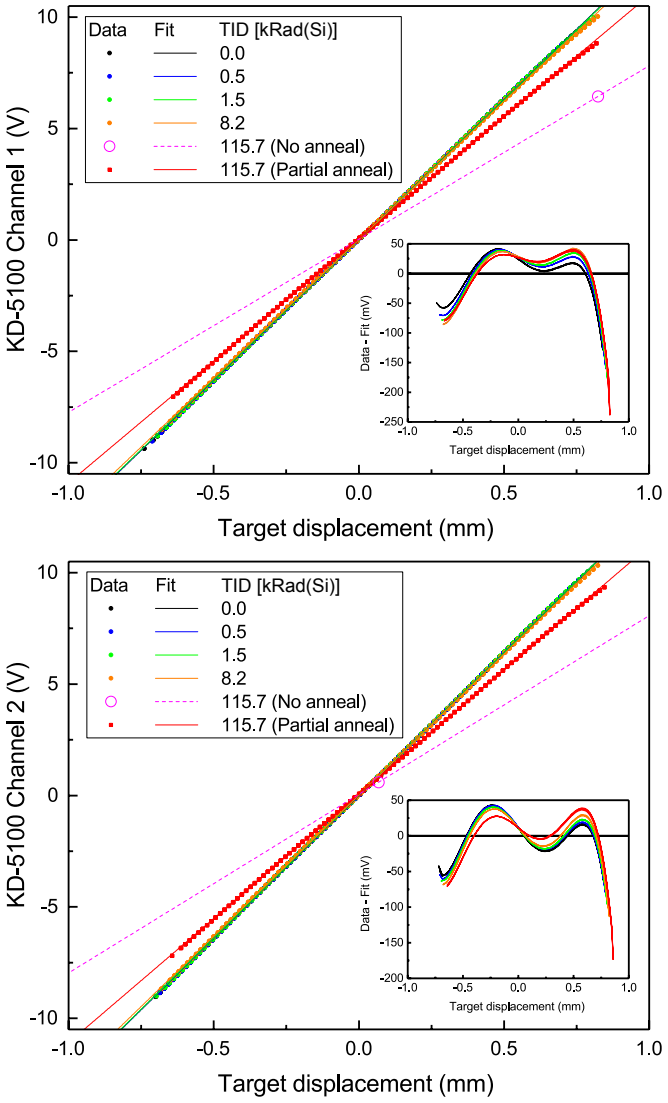

Fig. 3. Calibration data taken before, between, and after proton exposures. The x-axis values are inferred from the measured piezo-stage sensor outputs, with zero displacement chosen to match zero DUT output before all irradiation. The solid lines are linear fits of the form $V(x) = Gx + N$, with fit parameters listed in Table I. The dashed lines are estimated curves using data taken immediately after all exposure, assuming only the gain parameter G varies with irradiation. Insets show linear fit residuals (nonlinearities).

We exposed the electronics of the DUT in nine consecutive runs to proton irradiations with the flux and fluence profiles shown in Fig. 2. The proton beam was oriented normal to the plane of circuitry and entered through the thinner front of the DUT case. Before any exposure, we recorded an initial calibration data set. We then captured passive monitoring data sets for each beam exposure. Between some exposures, as indicated in Fig. 2, the monitoring data was interrupted in order to record additional calibration data sets. After the final beam exposure, we continued to record monitoring data to capture recovery behavior. During this time, we moved the DUT away from the beam so that proton testing of other

TABLE I

FIT PARAMETERS FOR CALIBRATION DATA IN FIG. 1, INCLUDING APPROXIMATE ELAPSED TIMES AND ANNEALING TIMES (SINCE THE END OF LAST EXPOSURE) AT THE BEGINNING OF CALIBRATION. VALUES IN PARENTHESIS ARE UNCERTAINTIES IN THE LAST DIGITS FROM LEAST-SQUARES FITTING OR ERROR PROPAGATION. THE PARAMETER $\Delta = |N - N_0| + |1 - G/G_0|(10\text{ V})$ IS AN ESTIMATE FOR THE WORST-CASE ERROR DUE TO IRRADIATION, WHERE N_0 AND G_0 ARE THE FIT PARAMETERS FOR 0 TID. THE ROW WITHOUT UNCERTAINTIES CORRESPONDS TO THE DASHED LINES IN FIG. 3.

Fluence	TID	Elapsed time	Anneal	KD-5100 Channel 1			KD-5100 Channel 2		
(10^{11} protons/cm^2)	[kRad(Si)]	(minutes)	(minutes)	G (V/mm)	N (mV)	Δ (V)	G (V/mm)	N (mV)	Δ (V)
0.00	0.00	−13	n/a	12.596(3)	0(1)	0.000	12.821(3)	0(1)	0.000
0.04	0.51	13	5	12.582(5)	−3(2)	0.014(4)	12.821(3)	2(1)	0.002(3)
0.12	1.54	34	4	12.563(5)	3(2)	0.029(5)	12.809(3)	11(1)	0.020(3)
0.61	8.17	67	4	12.409(6)	9(2)	0.157(5)	12.656(3)	20(2)	0.148(3)
8.66	115.70	113	0	7.775	36	3.863	8.017	51	3.798
8.66	115.70	374	261	10.948(4)	36(2)	1.344(4)	11.148(3)	51(1)	1.356(3)

components could be performed. We then recorded a final calibration before disassembling the test system.

III. EXPERIMENTAL RESULTS AND ANALYSIS

A. Calibration Data

Fig. 3 shows the calibration data. Linear fits to the data of the form $V(x) = Gx + N$ and corresponding fit residuals (nonlinearities) are shown, with fit parameters given in Table I. The data suggest that the effective gains G of each output channel decrease with irradiation. This decrease is presumably the result of gain degradation in amplifiers, which is a phenomenon known to occur in bipolar integrated circuits from both displacement damage and certain TID effects. We also observe the effective null N for each channel to change with irradiation. Using the fit parameters, we estimate a worst-case error Δ of the DUT performance from irradiation, which is shown in Table I. The error estimate Δ does not include the effects of the nonlinearities shown in Fig. 3, which we observe to slightly change with irradiation (this may be partly due to differing sweep ranges from technical offsets).

The calibration data is complicated by transient recovery behavior (or annealing), which we observe in monitoring data sets. This recovery behavior suggests that the worst-case error Δ shown is an overestimate for what would be observed in a space environment. Additionally, the data suggest that the error in practice from irradiation could be significantly reduced if the changes of the effective gain and/or null are mitigated, for example, by periodic re-calibration procedures for each channel.

B. Monitoring Data

Fig. 4 is an overview of the monitoring data for the channel outputs versus time, taken between the initial and final calibration measurements. The interruptions early in the data correspond to the calibration measurements indicated in Fig. 2. As mentioned earlier, the discontinuities at these interruptions are due to technical offsets, not proton exposure. The interruption later in the data corresponds to computer error. The final sequence of five exposures beginning near 72 min. were not interrupted by calibration measurements, and display annealing phenomenon after each exposure. This

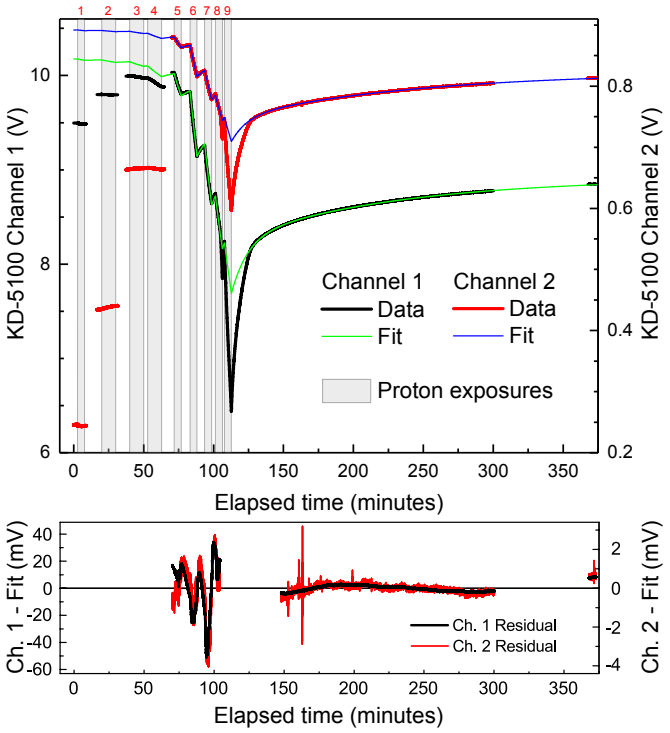

Fig. 4. (Top) Overview of monitoring data for the channel outputs. The value of both channels primarily decreased during exposure and increased afterwards. The three interruptions early in each data set correspond to calibration measurements, and the change in output values during these interruptions are dominated by technical offsets. The interruption late in each data set corresponds to computer error. Red numbers above grey regions label the exposure runs in Fig. 2. Finer detail of the monitoring data during exposure is shown in Fig. 5. (Bottom) Residuals for fits to the monitoring data using (1) with fit parameters listed in Table II. Data for the first four exposures were excluded because of technical offsets, as well as certain later data because of suspected thresholding effects, as explained in the text. Small spikes after 150 minutes are likely due to moving the DUT out of the beam path.

annealing is most evident after the final exposure concluded near 112 min., after which both channels show a decaying recovery tending towards saturation. The partial recovery seen in the data is consistent with trapped-hole annealing, displacement-damage annealing, or both. The changes in the DUT outputs are consistent with the gain degradation observed in the calibration measurements.

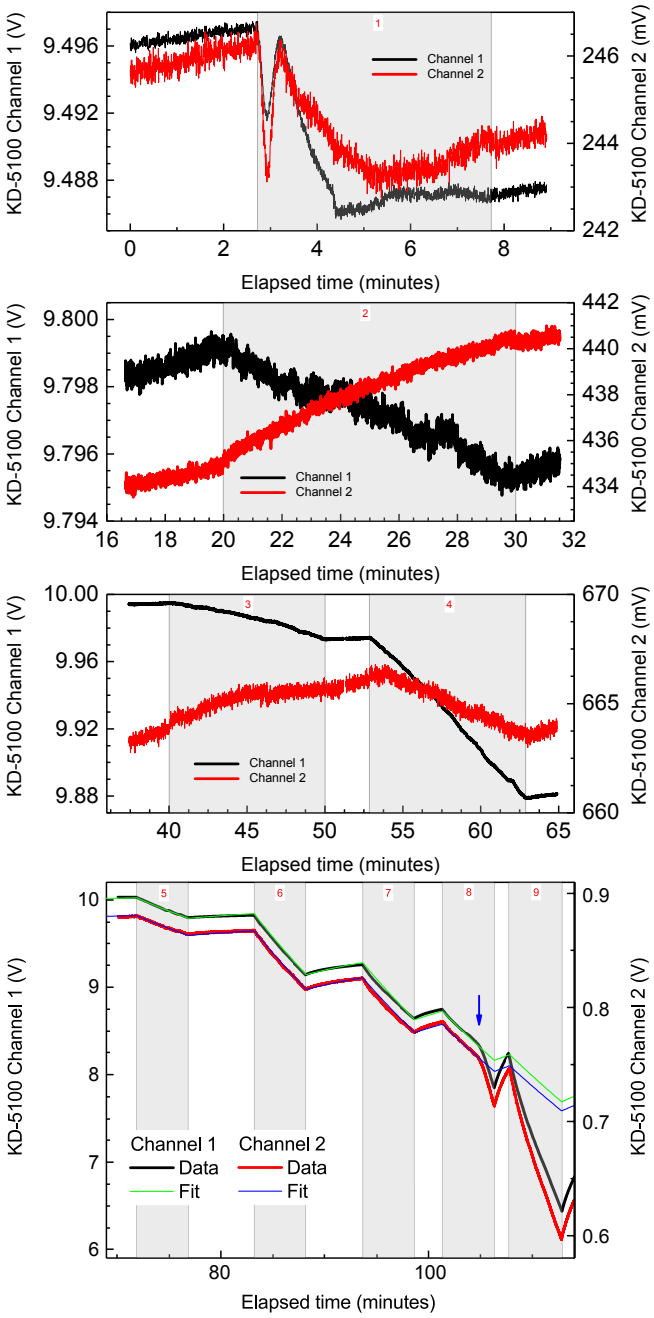

Fig. 5. Finer detail of monitoring data for the DUT outputs during irradiation. Red numbers and grey regions indicate exposure runs in Fig. 2. At the beginning of the first run, a similar oscillatory behavior was observed in both channels. While the overall trend was for both channel values to decrease during each exposure and increase afterwards, the value of the second channel increased during the second and third runs. The final panel highlights the similarity of both channels during runs five through nine. An arrow during the eighth exposure indicates the onset of suspected thresholding (nonlinearity), after which the response of both channels increased dramatically to radiation despite runs six through nine having similar flux and imparted fluence.

Additionally, Fig. 4 includes empirical fits to the monitoring data for the final five exposures using the model

$$V(t) = V_0 + A\,\Phi(t) + \sum_n B_n \int_{-\infty}^{t} \phi(\tau)\, e^{-(t-\tau)/T_n} d\tau, \quad (1)$$

with the flux $\phi(t)$ and fluence $\Phi(t)$ of Fig. 2, which gave the fit parameters in Table II. Here, the fit coefficient V_0 is an initial condition, A models static (degradation) effects, and each pair $\{B_n, T_n\}$ in the sum model the creation and exponential decay of independent dynamic (annealing) effects. This fitting excluded the initial four exposures because of technical offsets in the stage positions. Additionally, values below 8.4 V for channel 1 and 0.76 V for channel 2 were excluded because of suspected nonlinear (thresholding) effects: the responses of both axes increased dramatically towards the end of the eighth exposure below these voltages, as highlighted in Fig. 5. The linear form of (1) is unable to model such effects.

We chose the form of the empirical model (1) to attempt to separate degradation and annealing effects, and to enable estimates of the device response to flux $\phi(t)$ and fluence $\Phi(t)$ profiles different from those in Fig. 2. Note that each term of the sum in (1) is equivalent to the form of first-order reaction kinetics for the annealing of defects [6]. However, the form in (1) was modified to apply not only after periods of irradiation, but also during irradiation. To show this equivalence, note that if the dynamic change in voltage over time, $V(t) - V_0 - A\,\Phi(t) = \sum_n \beta_n [N_n](t)$, was a weighted sum over defect number densities $[N_n](t)$ with fixed coefficients β_n, and if $\phi(t) = 0$ for $t \geq 0$, then (1) would lead to $[N_n](t) = [N_n]_{t=0}\, e^{-k_n t}$ for each defect, which is equivalent to (2.56) of [6], with the parameters $[N_n]_{t=0} = (B_n/\beta_n) \int_{-\infty}^{0} \phi(\tau) e^{\tau/T_n} d\tau$ and $k_n = 1/T_n$.

The empirical fits in Fig. 4 describe the coarse response to irradiation well using only two terms in the sum ($n = 1, 2$), as shown by the fit residuals. However, care is required in using the model (1) and fit parameters in Table II to estimate the device response to different flux $\phi(t)$ and fluence $\Phi(t)$ profiles, because in addition to nonlinear thresholding at large fluence, we observe additional phenomenon in the fine response to irradiation that the empirical fits do not capture.

Fig. 5 shows the monitoring data during exposures in more detail. During the initial exposure, there was a small oscillatory response in both axes that the empirical fits of Fig. 4 do not capture. Additionally, the data for exposures 2 and 3 of the DUT channel 2 exhibit a direction of response that is opposite to that of the other channel and the empirical fits of Fig. 4. It is possible that this opposing response may be due to a gain sign flip after evolution through an amplification stage null in the device for axis 2, which used a stage position that produced an output near null. However, the technical stage offsets prevent a satisfactory analysis of this issue.

The bottom panel of Fig. 5 highlights the remarkable qualitative similarity of the responses of both DUT channels to the final five exposures. This suggests that the dominant form of radiation response may be from a shared component or circuit path between the otherwise independent channel circuitry. Furthermore, the onset of suspected thresholding is evident in both channels simultaneously: while the last four exposures had nearly the same flux and imparted fluence, the responses to irradiation changed markedly after the time indicated by an arrow in the panel. After this time, the data

TABLE II

FITS OF MONITORING DATA IN FIG. 4 USING (1) WITH THE FLUX $\phi(t)$ AND FLUENCE $\Phi(t)$ OF FIG. 2. VALUES IN PARENTHESIS ARE UNCERTAINTIES IN THE LAST DIGITS FROM LEAST-SQUARES FITTING. THE SHORTHAND $[\Phi] = 10^{12}$ PROTONS/CM^2 WHICH CORRESPONDS TO $\sim$ 134 KRAD(SI) TID.

Parameter:	V_0 (V)	A (V/[Φ])	B_1 (V/[Φ])	T_1 (minutes)	B_2 (V/[Φ])	T_2 (minutes)
KD-5100 Channel 1	10.1761(2)	−1.4586(7)	−1.920(3)	11.52(3)	−0.8749(5)	117.5(3)
KD-5100 Channel 2	0.891934(12)	−0.07899(6)	−0.1365(2)	11.10(3)	−0.09841(3)	134.5(2)

deviate significantly from the empirical fits until the values of channels 1 and 2 returned to above 8.4 V and 0.76 V, respectively, as shown in Fig. 4.

Fig. 6 shows the power supply currents versus time from the same monitoring data. The supply currents show a qualitatively similar behavior as the channel outputs in Fig. 4, decreasing during exposure and increasing afterwards. This behavior is consistent with gain degradation followed by partial recovery known to occur in current mirror sections of operational amplifiers. The sudden negative spikes observed after proton irradiation was completed are most likely due to moving the DUT out of the beam path and disturbing the test system to allow testing of other devices.

We did not observe any spikes or other anomalous behavior in the supply currents or the channel outputs during exposure, suggesting that the KD-5100 is insensitive to latchup or single event transients (SETs) from direct proton ionization as well as low linear energy transfer (LET) secondary particles. For incident protons with energies of 59 MeV, elastic collisions produce silicon recoils with a maximum energy of $\sim$ 8 MeV [7] and a corresponding maximum LET of 12 MeV-cm^2/mg and range of 4 μm. Inelastic spallation reactions will also contribute secondary particles, so these results suggest that the KD-5100 may exhibit reasonable tolerance to heavy ions [8]. However, testing in a heavy-ion beam is required to make a conclusive statement about heavy-ion effects, because of the short range of these secondary particles compared to the unknown, possibly large collection volumes that might be expected for older technology used in the KD-5100.

IV. CONCLUSION

We report 64 MeV proton testing of a Kaman KD-5100 system up to 8.6×10^{11} protons/cm^2 fluence and 115.7 kRad(Si) TID. We observed and characterized changes in KD-5100 performance with irradiation, and observed strong recovery characteristics. We presented a model to estimate the combined effects of degradation and annealing for different flux and fluence profiles. The data suggest that the KD-5100 will be suitable for space missions with low to moderate TID and displacement dose requirements, and possibly for missions with more challenging requirements depending on the position-measurement accuracy required. Further testing for enhanced low dose rate sensitivity (ELDRS) and heavy-ion effects and of additional KD-5100 samples is needed to understand the general behavior of KD-5100 systems in more challenging radiation environments.

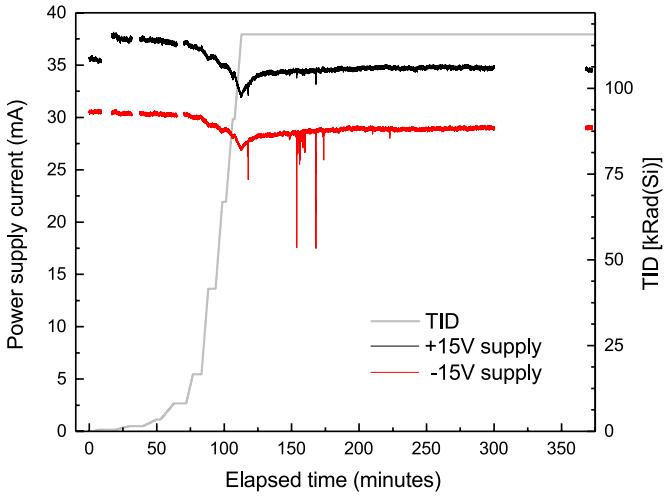

Fig. 6. DUT power supply currents and TID from proton irradiation as a function of time. The interruptions are from calibration measurements between exposures or computer error. Just like the channel outputs, the currents decreased with exposure and recovered afterwards. This behavior is consistent with gain degradation of bipolar circuits, which is known to result from both displacement damage and certain TID effects. The sudden dips after 110 minutes are most likely due to mechanical disturbances to the test system.

ACKNOWLEDGMENT

The authors are grateful to Terry Dillahunty and Dean Gacita of Kaman Aerospace Corporation for helpful discussions, Dominic Jandrain for software support, and Duane Drake for machining support.

REFERENCES

[1] Kaman Precision Products, "KD-5100 Data Sheet," [Online]. Available: http://www.kamansensors.com/html_pages/KD-5100.html, [Accessed July, 2017].

[2] G. C. Loney, "Design of a high-bandwidth steering mirror for space-based optical communications," *SPIE Active and Adaptive Optical Components*, vol. 1543, pp. 225–235, 1992.

[3] K. R. Lorell and J.-N. Aubrun, "Actively-supported multi-degree of freedom steerable mirror apparatus and method," US Patent 7 009 752, March 7, 2006.

[4] L. E. Hawe II, "Control of a fast steering mirror for laser-based satellite communication," Ph.D. dissertation, Massachusetts Institute of Technology, February 2006.

[5] Kaman Precision Products, "KD-5100 User Manual," [Online]. Available: http://www.kamansensors.com/html_pages/KD-5100.html, [Accessed July, 2017].

[6] F. Hönniger, "Radiation damage in silicon – defect analysis and detector properties," Ph.D. dissertation, Universität Hamburg, January 2008, Chapter 2.5.

[7] E. L. Petersen, "Single event analysis and prediction," *Notes from IEEE Nuclear and Space Radiation Effects Conference Short Course*, 1997, Snowmass, CO.

[8] E. Petersen, *Single Event Effects in Aerospace*. Piscataway: Wiley–IEEE Press, 2011, Chapter 8.